*Fibers and Polymers* 2019, Vol.20, No.2, 328-336
DOI 10.1007/s12221-019-8446-6

ISSN 1229-9197 (print version)
ISSN 1875-0052 (electronic version)

# Effects of STF and Fiber Characteristics on Quasi-Static Stab Resistant Properties of Shear Thickening Fluid (STF)-Impregnated UHMWPE/Kevlar Composite Fabrics

**Ting-Ting Li[1,2], Wenna Dai[1], Liwei Wu[1,2], Hao-Kai Peng[1,2], Xiayun Zhang[2], Bing-Chiuan Shiu[3], Jia-Horng Lin[1,2,3,4,5,6,7], and Ching-Wen Lou[1,4,6,7,8,9]***

[1]*Innovation Platform of Intelligent and Energy-Saving Textiles, School of Textile Science and Engineering, Tianjin Polytechnic University, Tianjin 300387, China*
[2]*Tianjin and Ministry of Education Key Laboratory for Advanced Textile Composite Materials, Tianjin Polytechnic University, Tianjin 300387, China*
[3]*Laboratory of Fiber Application and Manufacturing, Department of Fiber and Composite Materials, Feng Chia University, Taichung 40724, Taiwan*
[4]*Department of Chemical Engineering and Materials, Ocean College, Minjiang University, Fuzhou 350108, China*
[5]*Department of Fashion Design, Asia University, Taichung 41354, Taiwan*
[6]*School of Chinese Medicine, China Medical University, Taichung 40402, Taiwan*
[7]*College of Textile and Clothing, Qingdao University, Shandong 266071, China*
[8]*Department of Bioinformatics and Medical Engineering, Asia University, Taichung 41354, Taiwan*
[9]*Department of Medical Research, China Medical University Hospital, China Medical University, Taichung 40402, Taiwan*
(Received May 25, 2018; Revised November 14, 2018; Accepted November 15, 2018)

**Abstract:** In order to deeply explore the fiber characteristics influencing on stab resistance of shear thickening fluid (STF)-impregnated fabrics, two different weaving fabrics, ultra-high molecular weight polyethylene (UHMWPE) fabric and Kevlar fabrics are saturate the various concentrations and particle size of STFs. Result shows that, $SiO_2$/PEG-200 blends demonstrate quick shear-thickening property, and the critical shear rate lowers to 1.2-45 $s^{-1}$ with higher concentration of 75 nm $SiO_2$. STF concentration and particle size significantly affect spike puncture resistance property, but the knife stab resistance mainly depends on fiber characteristics. Comparatively, STF-UHMWPE composite fabrics exhibit better knife stab resistance but weaker spike puncture resistance than STF-Kevlar fabrics. This study can provide an optimization for structure design of stab resistance armors in the future.

**Keywords:** Stab resistance, Shear thickening fluid (STF), Rheology, Body armor

## Introduction

Stab-resistant clothing, as the human protective equipment, protects people from harming. However, the bulky and inflexibility of these conventional stab-resistant materials leads to inconvenient wear [1]. Therefore, it is an imperative goal for the researchers and manufacturers to develop lightweight, comfortable, flexible, and stab resistant clothing.

The shear thickening fluid (STF) is a kind of densely packed suspensions whose viscosity increases rapidly with the increasing of shear rate or shear stress. When subjected to high-speed impact, the STF transits from liquid to solid-like state and returns to the initial liquid state when the external force disappears [2,3]. Many domestic and foreign research institutes engage in research of STF for stab-resistant products. Inspired by Wagner's ideas, in-depth studies on the mechanical properties of Kevlar/STF were carried out. Experimental tests and numerical simulations show that Kevlar/STF has much better impact resistance than pure Kevlar fibers [4-7]. Lee *et al*. researched the ballistic impact characteristics of Kevlar fabrics impregnated with STF, and found that the addition of STF offers a significant enhancement in ballistic penetration resistance without losing flexibility [8]. Majumdar *et al*. demonstrated the deformation and energy absorption modes of STF-treated and untreated Kevlar woven fabrics upon impact, and found that in untreated Kevlar fabrics, only the primary yarns, participated in load sharing and hence energy absorption; however, for STF-treated fabrics, transformed STF acted as a bridging matrix which converts the network of yarns in the fabric into a single structure [9-12]. Park *et al*. also fabricated STF-treated high performance fabrics, and showed that STF treatment has a significant influence on protective performance of fabrics [13,14]. Baharvandi *et al*. studied the protective properties of STF impregnated fabric in quasi-static penetration. It was said that due to the increase of friction between yarns, STF treatment increases the energy absorption capacity of the fabric [15,16]. Haro *et al*. studied the ballistic behavior of hybrid composite laminates including STF impregnated high performance fabrics. Studies show that neat fabrics are more prone to be perforated in comparison to STF impregnated fabrics [17,18].

*Corresponding author: cwlou@asia.edu.tw

Similarly, domestic researchers have made an in-depth exploration of the fabric containing STF. Sun *et al*. [19] demonstrated that the stab-resistant property of UHMWPE sheets improved after they were impregnated with an STF. The stab resistance significantly increased as the mass fraction of silica in the STF was increased. The authors suggested that the optimal mass fraction of silica in STFs for knife and stab protection is 38 %. This study purposes to discuss effect of silica size on stab resistance properties of STF/UHMWPE. Liu *et al*. [20] examined the dynamic stab resistance properties of high performance UHMWPE fabrics impregnated with STF, and showed that the energy dispersion from STF/UHMWPE fabrics decreased with increase in the molecular weight of dispersing medium. In addition, the high performance fibers such as PBO and M-5 fibers [21-23] are also studied widely due to their excellent shear resistance. Jiang *et al*. [24] examined STF in terms of the application of stab resistant materials. They found that using STF effectively improved the stab resistance of Kevlar fabrics. Moreover, STF also improved the breaking strength in the same areal density, indicating that STF had valuable applications in the bulletproof and stab-proof fields. Moreover, the studies have accomplished achievement in terms of structure of stab-resistant materials, anti-stab mechanism, stab-resistant equipment, and computer simulation. Qiu *et al*. [25] discussed the properties of knitted body-armor-related fibers, i.e. Kevlar fibers and high performance PE fibers to apply on the body-armor materials. Song *et al*. [26] demonstrated that the impregnated STF improved the impact resistance performance of the Kevlar fabrics in terms of the impact energy absorption and the deformation. Especially, STF/Kevlar composites with spherical silica showed radial deformation behavior after impacted by the projectile, which was different from the neat Kevlar fabrics whose failure mode was fiber pull-out or fiber fracture.

Even that the studies on stab resistance of fabrics become mature, however, there are still a great number of problems of the development of stab-resistant clothing. The market is not standardized and materials have low safety and reliability. On the other hand, the stab mechanisms of stab-resistance armor when subjected to various sharp threats are different. During stab penetration, the human body is damaged from spike by fiber bundles penetration not fiber fracture. For knife stab, most of fibers is cut resulting in fabric damage. Therefore, fabric density and thickness as well as fiber characteristics play the important role to stab resistance properties [27].

Ultrahigh molecular weight polyethylene (UHMWPE) fabric has high impact resistance, but possesses excellent self-lubrication and small coefficient of friction between fibers, which results in UHMWPE easily shifted when suffering from spike and thus stab resistance decreased [28, 29]. Therefore, this study employs impregnation of STF with different size of silica (15 nm, 20 nm and 75 nm) and different proportions of STF (15 %, 20 %, 25 %) to increase the inter-fiber friction to improve stab resistance performance. Meanwhile, STF/UHMWPE are compared with pure aramid and STF/Kevlar fabrics, intended to analyze the influences of different fiber modulus as well as silica size and concentration on stab resistance properties. The optimizations design parameters of stab resistance armors are explored.

## Experimental

### Materials

Polyethylene glycol-200 (PEG-200) with chemical purity grade is purchased from Tianjin Xingfu Fine Chemical Research Institute, China. 15 nm, 20 nm and 75 nm fumed silica particles are provided from Guangzhou GBS high-tech & Industry Co. Ltd., China. Alcohol has purity of ≥99.7 % provided from Tianjin Fengchuan Chemical Reagent Technologies Co. Ltd., China. Kevlar filaments were supplied from DuPont Corporation. Ultra-high molecular weight polyethylene (UHMWPE) filaments are provided by Lianyungang Shente New Material Co., Ltd., China. The specifications of Kevlar and UHMWPE filaments are displayed in Table 1 respectively. The plain fabrics made by Kevlar and UHMWPE filaments are fabricated by a loom whose specification parameters are revealed in Table 2.

### Preparation of Shear Thickening Fluid (STF), STF-UHMWPE and STF-Kevlar Composite Fabrics

The STF is made as the process shown in Figure 1. PEG-200 serves as the dispersion medium. 15 nm, 20 nm and 75 nm fumed silica ($SiO_2$) particles serve as the dispersed particles. $SiO_2$ and PEG-200 at mass ratios of 4.5:25.5, 6:24, and 7.5:22.5 are blended to form STF of concentrations of 15 %, 20 %, and 25 %. PEG blended with $SiO_2$ by a mechanical stirrer at an initial rate of 100 rpm. When the designated amount of $SiO_2$ is totally infused, the stirring rate is increased to 600 rpm for totally blending. After ultrasonic oscillation for 5 hrs, $SiO_2$ evenly dispersed in PEG. The

**Table 1.** Physical properties of Kevlar and UHMWPE filaments

| | Aramid yarn | UHMWPE filament |
|---|---|---|
| Fineness (tex) | 58 | 63 |
| Tensile strength (MPa) | 1020 | 2000 |
| Tensile modulus (GPa) | 65 | 80 |
| Elongation at break (%) | 2.4 | 3.1 |

**Table 2.** Specifications of the fabric

| | Aramid | UHMWPE |
|---|---|---|
| Structure | Plain weave | Plain weave |
| Density (inch) | 32×32 | 28×28 |
| Weight ($g/m^2$) | 176 | 170 |

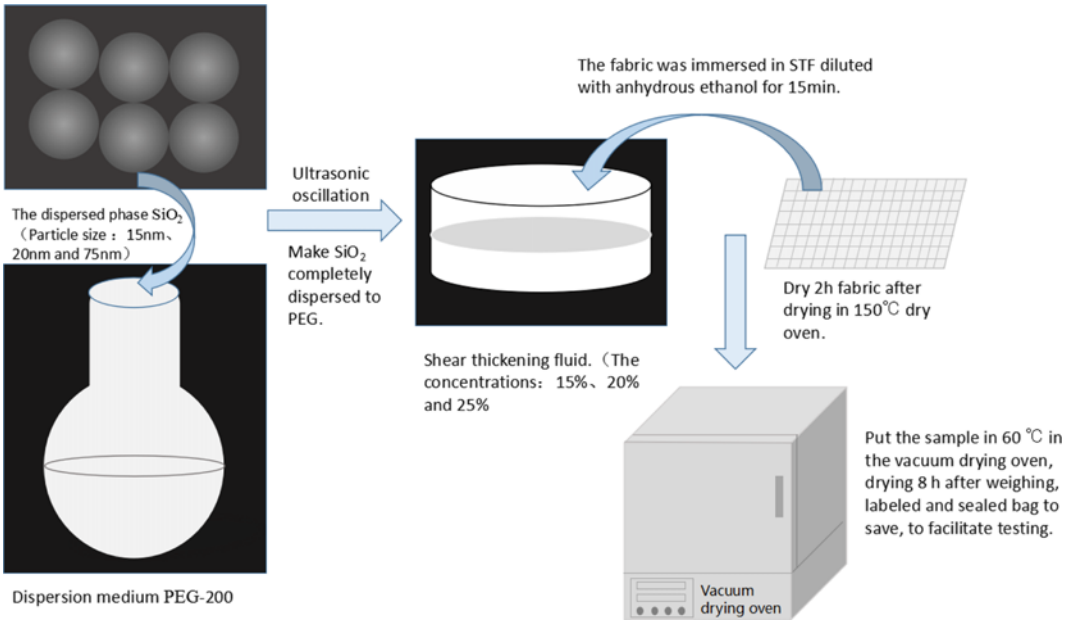


**Figure 1.** Preparation process of Shear thickening fluid (STF) and STF-impregnated composite fabric.

obtained blends then kept in a vacuum drying oven at 60 °C for 24 hrs in order to remove the bubbles and obtain the evenly dispersed and stabilized STF systems [13-15]. STF and anhydrous ethanol are blended at a ratio of 1:1 for dilution to facilitate the combination of STF and fabrics [30-32]. UHMWPE fabrics and Kevlar fabrics are trimmed to the size of 10 cm×10 cm, and are separately immersed in a diluted STF. The fabrics that fully absorb STF are dried in vacuum drying oven at 60 °C for 30 minutes, forming the STF-UHMWPE and STF-Kevlar composite fabrics (Figure 1).

## Characterization

### *Rheology Measurement*

According to the rotary rheometer (Bohlin CVO type, Malvern Instruments Co., Ltd., UK), the rheological properties of STF was measured. Rheological properties indicate the relationship between the system viscosity (η) and the shear rate (γ). The flat rotor has a diameter of 40 mm, the distance between the upper and lower plates is 0.3 mm, and the shear rate is between 0.1-1000 $s^{-1}$ [5,30].

### *Anti-Stab Performance Test*

According to ASTM F1342-05, STF/UHMWPE and STF/Kevlar composites were tested by Instron 3369 (Instron, USA). The head (*i.e.* a spike or a knife) that was attached to the load cell individually penetrated the samples at a constant rate of 200 mm/min. The dimensions of spike and knife were displayed in Figure 3. The fixture specifications of testing samples were shown as Figure 4.


**Figure 2.** Bohlin CVO Rotary rheometer.

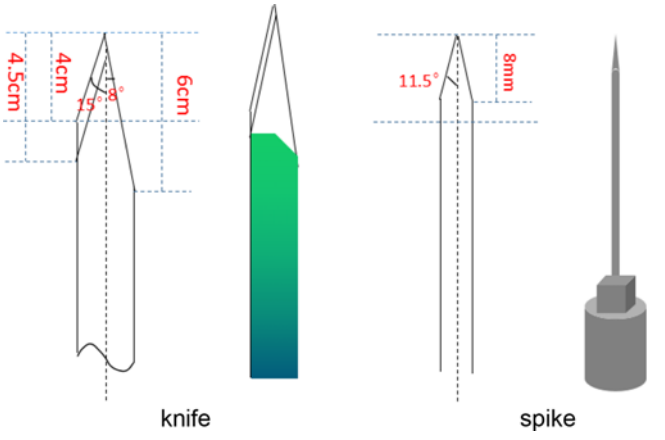


**Figure 3.** Specifications of the knife and spike.

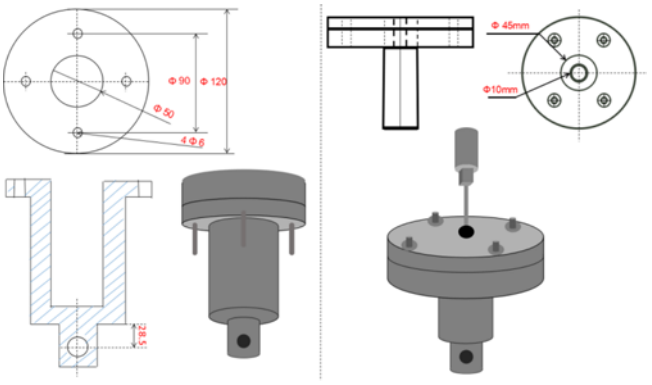

**Figure 4.** Fixture specifications and parameters.

## Results and Discussion

### Rheological Properties of STF

#### *Effect of Particle Size*

Figure 5 shows the viscosity (η)/shear rate (γ) curves of the $SiO_2$/PEG200 dispersion system at 25 °C with the concentration of $SiO_2$ being 15 % (Figure 5(a)), 20 % (Figure 5(b)), and 25 % (Figure 5(c)) and $SiO_2$ particle size being 15 nm, 20 nm, and 75 nm. With a specified concentration of $SiO_2$, the dispersion system is typical and shows good shear thickening properties regardless of whether the particle size being 15, 20, and 75 nm. At low shear rate, the viscosity of the dispersion system decreases as the shear rate increases, causing the thinning shear effect. When shear rate increases to the critical value, the viscosity of the dispersion system increases and the shear is thickened. This trend is highly consistent with literatures [31,32].

There are different rheology properties based on the combinations of parameters. In Figure 5(a), the initial viscosity, 4.11 Pa·s, is much lower than that of similar studies about STF that contained 55 % 15 nm $SiO_2$ (>10 Pa·s) [33], which demonstrates that $SiO_2$ content has very significant influence on rheological properties. In general, initial viscosity of STF system decreases as a result of increasing the particle size of $SiO_2$. The initial viscosity values are 3.88 Pa·s (75 nm), 9.92 Pa·s (20 nm) and 35.43 Pa·s (15 nm) respectively for 20 %-$SiO_2$/PEG200 systems (see Figure 5(b)), and 6.59 Pa·s (75 nm), 18.81 Pa·s (20 nm) and 65.43 Pa·s (15 nm) respectively for 25 %-$SiO_2$/PEG200 in Figure 5(c). It can be also seen that with the same particle size, the corresponding initial viscosity value is increased by about 2 times as STF concentration increases. This result may be ascribed to the interspace between particles in Figure 6. As given the same mass ratios of $SiO_2$ and PEG, small $SiO_2$ particle size means the number of particles is high and the distance between particles is small (see Figure 6), which decreases the mobility and yields a high initial viscosity. With the increase in shear rate, the particles in the dispersion system collide drastically, and also different numbers and

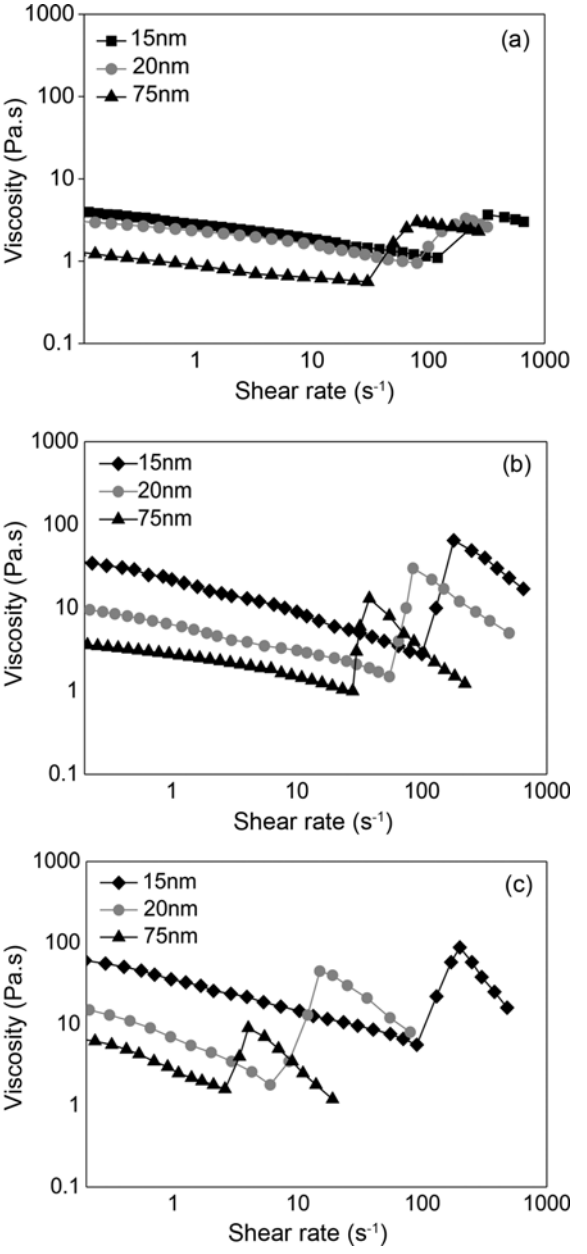


**Figure 5.** Rheological behavior of STF as related to particle size and concentration of $SiO_2$ particles; (a) 15 %-$SiO_2$/PEG200, (b) 20 %-$SiO_2$/PEG200, and (c) 25 %-$SiO_2$/PEG200.

sizes of particle clusters are formed after overcoming the gravity of particles themselves and repulsion force between particles. These particle clusters increase the friction between the fibers, thereby increasing the fabric tightness and areal density, and also makes the textiles rougher [34], resulting in improvement of the spike puncture resistance. In addition, addition of the spatial network structure of $SiO_2$ particles (see Figure 7) increases the wear resistance of the fabric thereby improving the knife stab resistance [35,36].

Macroscopically, the STF exhibits a thickening phenomenon.

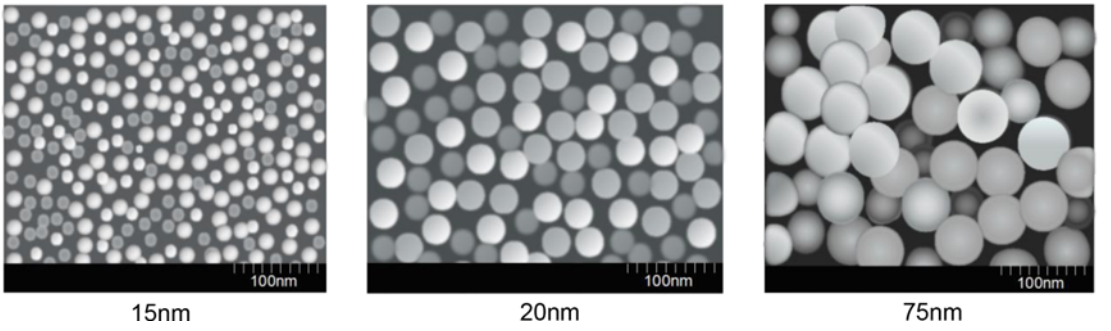


**Figure 6.** The morphological of voids between particles.

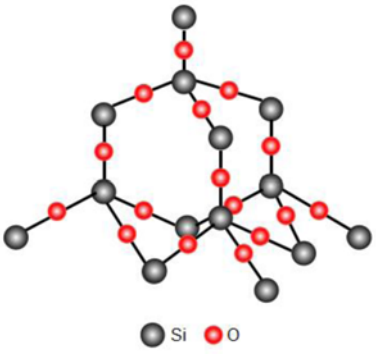


**Figure 7.** Spatial network structure of $SiO_2$ particle.

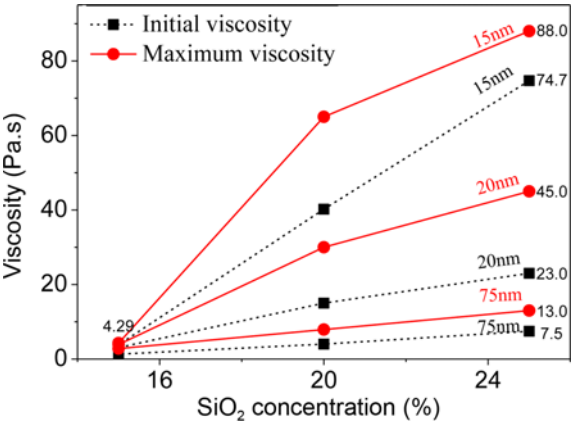


**Figure 8.** Initial viscosity and maximum viscosity curve of $SiO_2$/PEG200 system at different mass ratios.

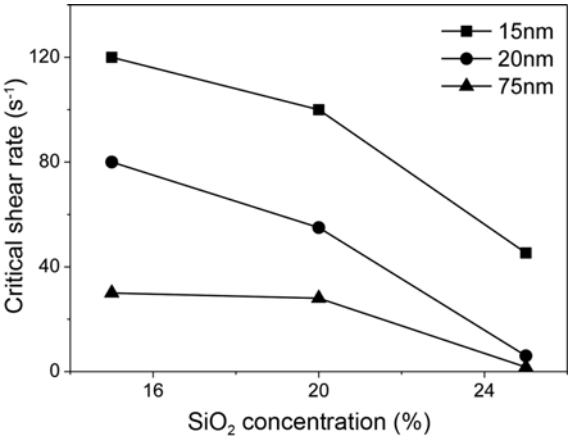


**Figure 9.** Curve of critical shear rate of $SiO_2$/PEG200 system at different mass ratios.

After the system becomes thickened, the maximum viscosity decreases when the particle size increases. A large size of $SiO_2$ particles means a small number of particles. As a result, the number of the particle clusters decreases, which sabotages the reaction between the particle clusters and eventually decreases the maximum viscosity of the dispersion system [37]. In sum, small $SiO_2$ particles lead to a greater critical shear rate as they require a higher shear rate to balance the hydration and repulsion between particles, which in turn thickens the shear based on the particle cluster theory [5, 38].

***Effect of Particle Concentration***

Figure 8 shows the initial and maximum viscosities of $SiO_2$/PEG200 dispersion system based on different ratios of $SiO_2$ and PEG. The higher the mass ratio of $SiO_2$, the higher the initial and maximum viscosities. For 15 nm-$SiO_2$ STF system, the initial and maximum viscosity values are both increased by about 20 times from 15 % to 25 % concentration. The maximum viscosity is slightly greater than the initial viscosity at a low concentration of $SiO_2$, and the thickening effect is not obvious. Increasing the concentration of $SiO_2$ makes the maximum viscosity higher than initial viscosity, and the system shows an obvious thickening effect. But shear thickening effect is not apparent when STF containing coarser $SiO_2$. This phenomenon can be still explained by the Particle Cluster Theory [39]. Similarly, increasing the concentration of $SiO_2$ significantly decreases the critical shear rate as displayed in Figure 9 and Table 3. Therefore, a high concentration of disperse phase (*i.e.* $SiO_2$) results in a more apparent thickening effect, and a high mass

**Table 3.** The shear rate critical value of STF

| | 15 nm | | | 20 nm | | | 75 nm | | |
|---|---|---|---|---|---|---|---|---|---|
| Critical shear rate ($s^{-1}$) | 15 % | 20 % | 25 % | 15 % | 20 % | 25 % | 15 % | 20 % | 25 % |
| | 120.00 | 100.00 | 45.30 | 80.00 | 55.00 | 6.00 | 30.00 | 27.99 | 1.70 |

ratio of $SiO_2$ is required when a low shear rate is used for the thickening process.

**Spike Puncture Resistance Property**

Stab resistance of STF-UHMWPE composite fabrics depends on two factors. The first was the hardness of $SiO_2$ and friction between fibers [24]. For spike puncture, the inter-yarn friction is the main influencing factors. During spike puncture process, yarn can be pulled out followed with spike penetration, which can change the compactness of the fabric and increase the inter-yarn friction.

Figure 10 shows the spike puncture resistance of STF-UHMWPE composite fabrics as related to different $SiO_2$ particle size and concentration of $SiO_2$ particle. With a specified concentration of $SiO_2$ particles, the larger the particle size, the lower the maximum compression load of STF-UHMWPE composite fabrics. When STF concentration was 25 % and size of $SiO_2$ was 15 nm, the maximum compression force of STF-UHMWPE (120.98 N) is increased by 2.7 times than pure UHMWPE fabrics (44.98 N). This is because the inter-yarn friction mainly affects spike stab and STF-immersion affects inter-yarn friction. The trends of compression force varied with $SiO_2$ size and concentration has a certain relation to STF rheological property. In the PEG200, the smaller size of $SiO_2$ and higher concentration of STF generates better viscosity and rheological performance. Shorter average distance between particles attributes to high possibility for mutual interference and collusion between particles and to high viscosity, and thus the mobility of particles is restricted more easily as indicated in literature [39]. When a shear forced is exerted, the high mobility resistance and obvious shear thickening effect contribute to high stab and puncture resistances. Although the larger size of $SiO_2$ agglomerated under the shear force, the space of particles-particles is large enough to accommodate smaller particles, which cannot cause the shear thickening phenomenon and makes fluid concentration decreased. Especially at a certain concentration, as the size of the $SiO_2$ particles increases, the number of particles in the fluid system decreases and particles clusters is also formed difficultly, which makes the interaction between the clusters and maximum viscosity both decreased. Therefore, compared to the smaller $SiO_2$ particle, the friction between the fibers in the fabric is reduced and stab resistance is lowered. However, one benefit for the larger particle size is that if critical shear rate cannot be adjusted by mono-sized particles, more diversified particle sizes can adopt for the desired rheological parameters [40, 41].

Figure 11 shows the spike puncture resistance of STF-Kevlar composite fabrics as related to different $SiO_2$ particle size and concentration of $SiO_2$ particles. The maximum compressive load, 136.50 N, occurs when the particle size is 15 nm and the concentration of the particle is 25 %. This value is increased by 3.4 times compared to pure Kevlar fabrics (40.63 N). The stab resistance mechanism is similar to STF-UHMWPE composite fabrics. Namely, at higher concentration of $SiO_2$ in the STF system, the number of dispersion particles becomes higher with the same size of $SiO_2$ particle, and meanwhile the inter-distance between particles becomes narrow. Under external force, the disperse particles easily form cluster and occurs shear thickening

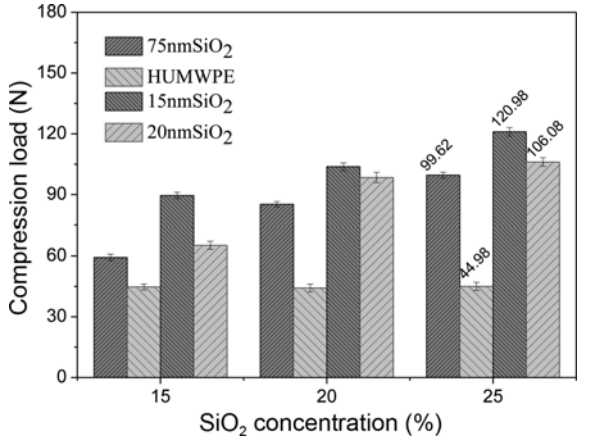


**Figure 10.** Spike puncture test of STF/HUMWPE composite fabric as related to particle size and concentration of $SiO_2$ particles.

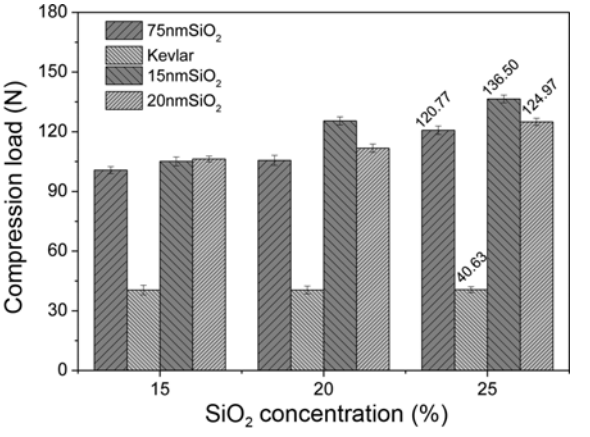


**Figure 11.** Spike puncture test of STF/Kevlar composite fabric as related to particle size and concentration of $SiO_2$ particles.

[39]. In addition, the smaller size of $SiO_2$ can prepare into more uniform STF suspension. But the UHMWPE fiber has good flexibility and exhibits good mechanical properties at high strain rate, and thus the UHMWPE fiber bears higher impact velocity than Kevlar fibers [37,42].

**Knife Stab Resistance Property**

The blade has continuous cutting edges that result in longer cutting area, and the stab damage thus has a higher destructive effect than that caused by the puncture damage [24]. Figure 12 shows the knife stab resistance of STF-UHMWPE composite fabrics made of different $SiO_2$ particle sizes and concentration of $SiO_2$ particles. STF-UHMWPE composite fabrics have the maximum stab resistance, 75.70 N, when the concentration of $SiO_2$ particles is 25 % and the particle size is 15 nm. Compared to pure UHMWPE fabric (45.22 N), the maximum compression force is improved by 1.7 times. This is due to the fact that silica particles agglomerated fast into solid-like substance, which limits the movement of the fibers and makes the knife stab pierced fabric difficultly [43]. Besides, the shear thickening phenomenon also can be described by the transition of the particles' microstructure from an equilibrium state (which has been established through the repulsive Brownian force) to a flocculated (agglomerated) state [37,43]. In contrast to Figure 10, knife compression force of STF-UHMWPE is decreased. The main reason is from different stab mechanism. Knife stab is from the fiber cut and thus the fiber strength and toughness are not improved even after STF impregnation.

Figure 13 shows that unlike the puncture curve that is smooth, the knife stab curve of STF/UHMWPE composite fabrics fluctuates significantly and the compressive load first increases and then decreases. This result is due to the angle that the single blade is held as seen in Figures 3. Due to the difference in the angle of the blade and its back, the contact angle between the blade and the sample continuously changes as a result of the successive piercing by the blade and the fibers demonstrate the corresponding breakages, which sabotages the fabrics [24].

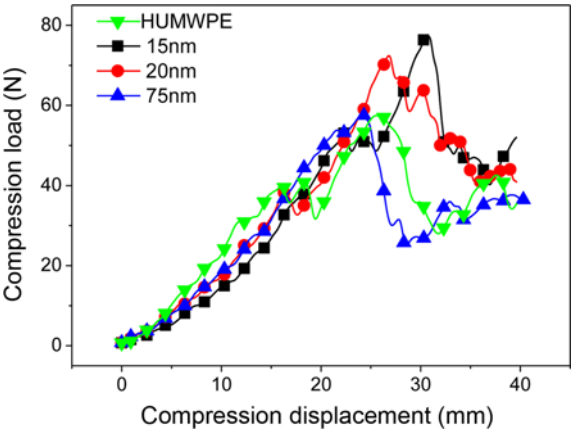


**Figure 13.** Knife stab test curves of STF/ UHMWPE composite fabrics saturated in a 25 % STF.

Figure 14 shows the knife stab resistance of STF-Kevlar composite fabrics as related to different $SiO_2$ particle size and concentration of $SiO_2$ particles. STF-Kevlar composite fabrics have the maximum stab resistance, 66.89 N, when the concentration of $SiO_2$ particles is 25 % and the particle size is 15 nm. This maximum value is increased by 1.3 times compared to pure Kevlar fabrics (40.63 N). The knife stab resistance of STF-Kevlar composite fabrics is lower than that of STF-UHMWPE composite fabrics. This is because aramid fibers have lower modulus than UHMWPE fiber as displayed in Table 1, and when the aramid fabric used as the carrier, the knife stab resistance of the STF-Kevlar composite fabric is not as good as the STF-UHMWPE composite as demonstrated by Li *et al.* [44].

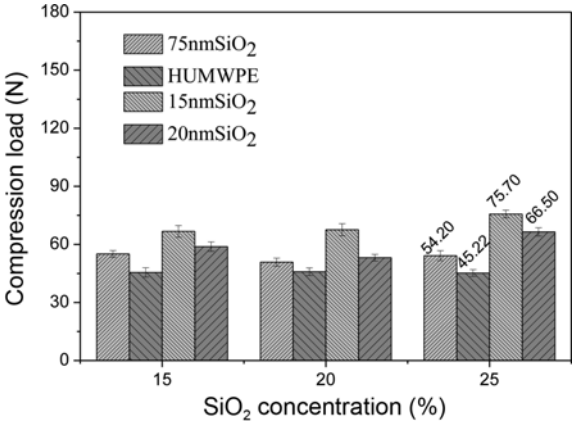


**Figure 12.** Knife stab test of STF/UHMWPE composite fabrics made of different $SiO_2$ content and particle size.

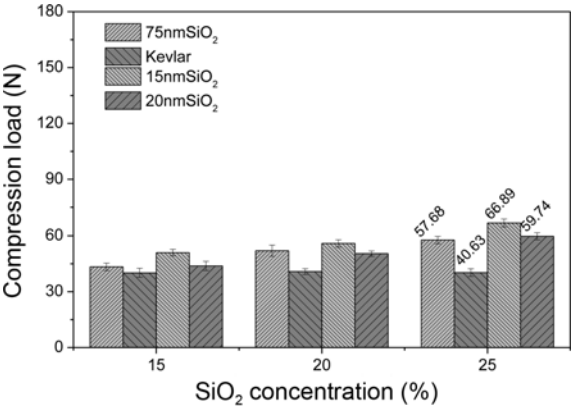


**Figure 14.** Stab resistance of STF/aramid composite fabrics made of different concentration of $SiO_2$ and $SiO_2$ particle sizes.

## Conclusion

In this study, the stabilized and uniform STF systems are formed by PEG 200 as dispersion medium and $SiO_2$ particles as dispersion phase using mechanical stirring and ultrasonic oscillation. After Kevlar and UHMWPE fabrics are separately immersed in the STF, the STF/UHMWPE and STF/Kevlar composite fabrics are prepared for rheology and puncture/stab resistance tests. Effects of $SiO_2$ particles and STF concentration on rheology of STF systems and puncture/stab resistance of STF/UHMWPE and STF/Kevlar composite fabrics are explored.

Within a specific concentration, $SiO_2$/PEG200 system has a good shear thickening effect regardless of particle sizes of 15, 20, or 75 nm. However, as $SiO_2$ particle size increases, the initial viscosity, critical viscosity and the maximum viscosity of SiO2/PEG200 systems decreases. At a specific particle size, the critical shear rate of SiO2/PEG200 system decrease with increment in concentrations of particles. Therefore, lower shear rate of STF happens at higher concentration and smaller size of $SiO_2$. Knife stab and spike puncture has different stab mechanism, which results in higher knife stab resistance for STF-UHMWPE composite fabrics and higher spike puncture resistance for STF-Kevlar composite fabrics. In particular, the optimal stab/puncture resistance of STF-UHMWPE and STF-Kevlar composite fabrics occurs when $SiO_2$ particle size is 15 nm and concentration of $SiO_2$ particles is 25 %.

To a large extent, STF impregnation cannot improve the fiber's strength and toughness effectively; therefore, the knife stab resistance exhibited not better than spike stab resistance for both of STF-UHMWPE and STF-Kevlar composite fabrics. In the following study, we will further systematically study the improvement of knife stab resistance and energy absorption capacity of STF-impregnated fabrics by particle surface modification and fabric textures design.

## Acknowledgements

The authors gratefully acknowledge the financial support provided by the Natural Science Foundation of Tianjin (18JCQNJC03400), the National Natural Science Foundation of China (grant numbers 51503145, 11702187, 11502163), and the Natural Science Foundation of Fujian (2018J01504, 2018J01505). This study is also supported by the Opening Project of Green Dyeing and Finishing Engineering Research Center of Fujian University (2017001A, 2017002B, 2017003B and 2017005B) and the Program for Innovative Research Team in University of Tianjin (TD13-5043).

## References

1. A. Johnson, G. A. Bingham, and D. I. Wimpenny, *Rapid. Prototyping. J.*, **19**, 199 (2013).
2. H. A. Barnes, *J. Rheol.*, **33**, 329 (1999).
3. E. Brown and H. M. Jaeger, *Rep. Prog. Phys.*, **77**, 046602 (2014).
4. A. Haris, H. P. Lee, T. E. Tay, and V. B. C. Tan, *Int. J. Impact. Eng.*, **80**, 143 (2015).
5. T. A. Hassan, V. K. Rangari, and S. Jeelani, *Mater. Sci. Eng. A.*, **527**, 2892 (2010).
6. Y. Park, Y. H. Kim, A. H. Baluch, and C. G. Kim, *Int. J. Impact. Eng.*, **72**, 67 (2014).
7. Y. Park, Y. H. Kim, A. H. Baluch, and C. G. Kim, *Compos. Struct.*, **125**, 520 (2015).
8. Y. S. Lee, E. D. Wetzel, and N. J. Wagner, *J. Mater. Sci.*, **38**, 2825 (2003).
9. A. Majumdar, B. S. Butola, and A. Srivastava, *Mater. Des.*, **51**, 148 (2013).
10. A. Majumdar, B. S. Butola, and A. Srivastava, *Mater. Des.*, **46**, 191 (2013).
11. A. Majumdar, B. S. Butola, and A. Srivastava, *Mater. Des.*, **54**, 295 (2014).
12. A. Srivastava, A. Majumdar, and B. S. Butola, *Mater. Sci. Eng. A.*, **529**, 224 (2011).
13. J. L. Park, B. I. Yoon, J. G. Paik, and T. J. Kang, *Text. Res. J.*, **82**, 527 (2012).
14. J. L. Park, B. I. Yoon, J. G. Paik, and T. J. Kang, *Text. Res. J.*, **82**, 542 (2012).
15. H. R. Baharvandi, M. Alebooyeh, M. Alizadeh, P. Khaksari, and N. Kordani, *J. Ind. Text.*, **46**, 473 (2015).
16. H. R. Baharvandi, M. Alebooyeh, M. Alizadeh, M. S. Heydari, N. Kordani, and P. Khaksari, *J. Exp. Nanosci.*, **11**, 550 (2015).
17. E. E. Haro, A. G. Odeshi, and J. A. Szpunar, *Int. J. Impact. Eng.*, **96**, 11 (2016).
18. E. E. Haro, J. A. Szpunar, and A. G. Odeshi, *Compos. Part. A-Appl. S.*, **87**, 54 (2016).
19. L. L. Sun, D. S. Xiong, and C. Y. Xu, *J. Appl. Polym. Sci.*, **129**, 1922 (2013).
20. W. Li, D. Xiong, X. Zhao, L. Sun, and J. Liu, *Mater. Des.*, **102**, 162 (2016).
21. W. Zhang and Z. Zheng, *Wool. Text. J.,* **3**, 24 (2005).
22. S. Bourbigot and X. Flambard, *Fire. Mater*, **26**, 155 (2002).
23. M. Lammers, E. A. Klop, M. G. Northolt, and D. J. Sikkema, *Polymer,* **39**, 5999 (1998).
24. X. Gong, Y. Xu, W. Zhu, S. Xuan, W. Jiang, and W. Jiang, *J. Compos. Mater.,* **48**, 641 (2014).
25. G. X. Qiu and Y. M. Jiang, *Knitting. Industries*, **2**, 62 (2003). (In Chinese)
26. H. S. Song , B. I. Yoon, C. Y. Kim, J. L. Park, and T. T. Kang, *Compos. Res.*, **20**, 1 (2007).
27. D. T. Tien, J. S. Kim, and H. You, *Fiber. Polym.*, **12**, 808 (2011).
28. C. Y. Huang, J. Y. Wu, C. S. Tsai, K. H. Hsieh, J. T. Yeh, and K. N. Chen, *Surf. Coat. Tech.*, **231**, 507 (2013).
29. Y. Wang, Z. Yin, H. Li, and G. Gao, *Wear*, **380**, 42 (2017).

30. T. J. Kang, Y. K. Chang, and K. H. Hong, *J. Appl. Polym. Sci.*, **124**, 1534 (2012).
31. H. R. Baharvandi, P. Khaksari, N. Kordani, M. Alebouyeh, M. Alizadeh, and J. Khojasteh, *Fiber. Polym.*, **15**, 2193 (2014).
32. T. J. Kang, K. H. Hong, and R. Y. Mi, *Fiber. Polym.*, **11**, 719 (2010).
33. T. A. Hassan, V. K. Rangari, and S. Jeelani, *Ultrason. Sonochem.*, **17**, 947 (2010).
34. L. H. Xu, Y. Shen, Y. Ding, and L. M. Wang, *J. Nanosci. Nanotechnol.*, **18**, 6879 (2018).
35. M. Wu, Y. Wang, and M. Wang, *Fibres Text. East. Eur.,* **16**, (2008).
36. Y. Wang, Y. Zhu, and X. Fu, *Text. Res. J.*, **85**, 980 (2015).
37. F. J. Galindo-Rosales, F. J. Rubio-Hernández, and J. F. Velázquez-Navarro, *Rheol. Acta*, **48**, 699 (2009).
38. S. Gürgen and M. C. Kuşhan, *Compos. Part A-Appl. S.*, **94**, 50 (2017).
39. H. L. Yang, J. M. Ruan, Q. M. Wu, Z. C. Zhou, and J. P. Zou, *Acta. Phys-Chim. Sin.*, **24**, 433 (2008).
40. S. Gürgen, M. C. Kuşhan, and W. Li, *Korea-Aust Rheol J.*, **28**, 121 (2016).
41. M. J. Decker, C. J. Halbach, and C. H. Nam, *Compos. Sci. Technol.,* **67**, 565 (2007).
42. X. Zhang and Y. Wang, *Polym. Bull.*, **70**, 821 (2013).
43. H. L. Yang, J. M. Ruan, Z. C. Zhou, J. P. Zou, Q. M. Wu, and Y. Y. Yan, *J. Cent. South. Univ.,* **16**, 926 (2009).
44. C. S. Li, X. C. Huang, Y. Li, N. Yang, Z. Shen, and X. H. Fan, *Polym. Advan. Technol.*, **25**, 1014 (2015).